Supporting Information

Growth modulation of nonlayered 2D-MnTe and MnTe/WS_2 heterojunction for high-performance photodetector

Taikun Wang[a,b], Fapeng Sun[a,b,c], Wenting Hong[a,b], Chuanyong Jian[a,b], Qinkun Ju[a,b,c], Xu He[a,b], Qian Cai[a,b], Wei Liu[a,b]**

[a]CAS Key Laboratory of Design and Assembly of Functional Nanostructures, and Fujian Provincial Key Laboratory of Nanomaterials, Fujian Institute of Research on the Structure of Matter, Chinese Academy of Sciences, Fuzhou, Fujian, 350002, China

[b]Fujian Science & Technology Innovation Laboratory for Optoelectronic Information of China, Fuzhou, Fujian 350108, P. R. China

[c]University of Chinese Academy of Sciences, Beijing, 100049, China

E-mail:hexu@fjirsm.ac.cn, liuw@fjirsm.ac.cn

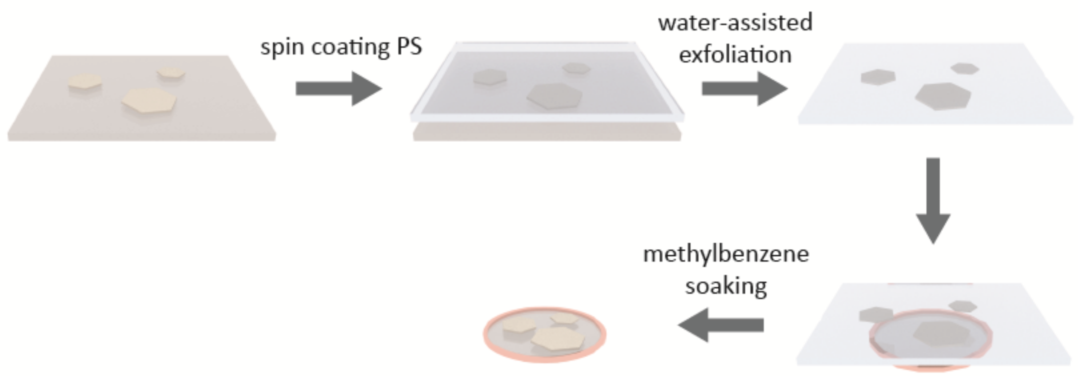

Figure S1. Schematic diagram of the process to transfer MnTe nanosheets onto a copper mesh.

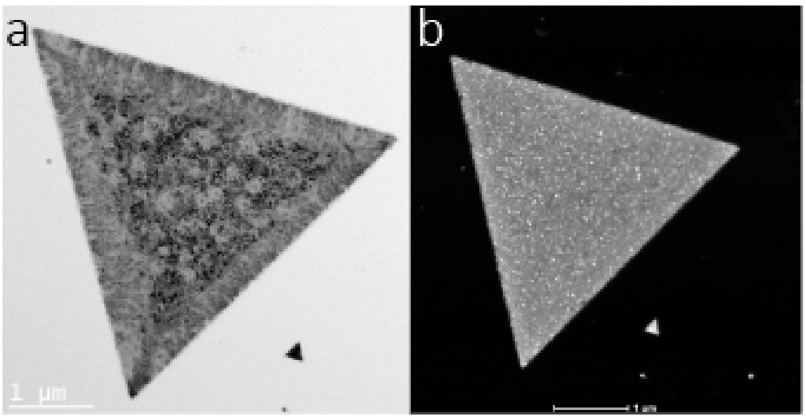

Figure S2. Low-magnification transmission electron microscopy images (a) and high-angle annular dark-field (HAADF) image (b) of MnTe nanosheet.

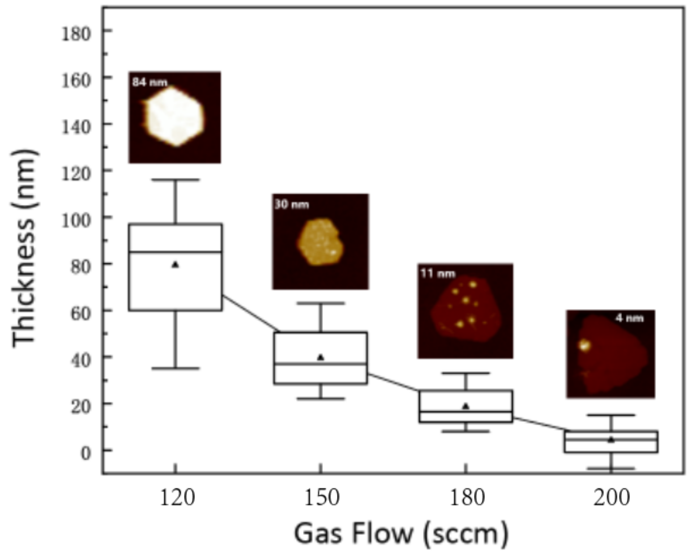

Figure S3. The average thickness of MnTe nanosheets grown at different gas flows.

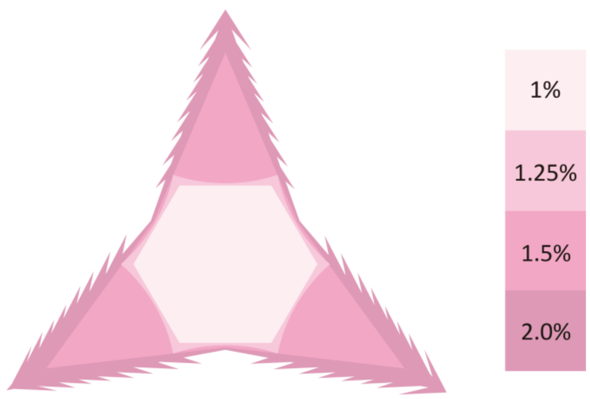

Figure S4. Morphological evolution of MnTe nanosheets as single-domain net growth rate increases.

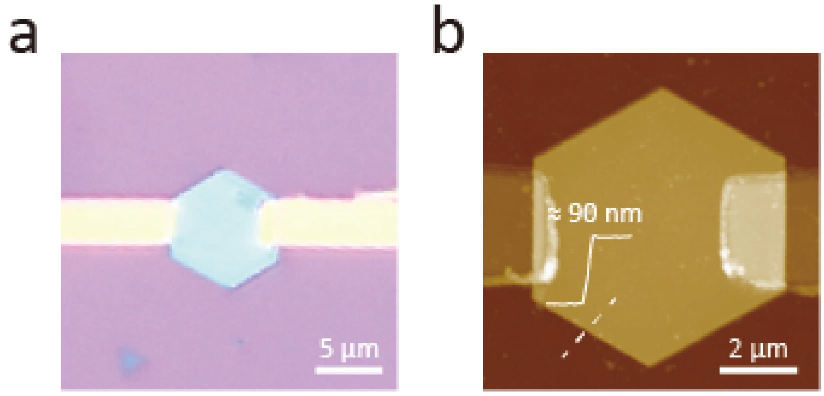

Figure S5. The optical microscopy image (a) and the AFM image (b) of MnTe-based FET device.

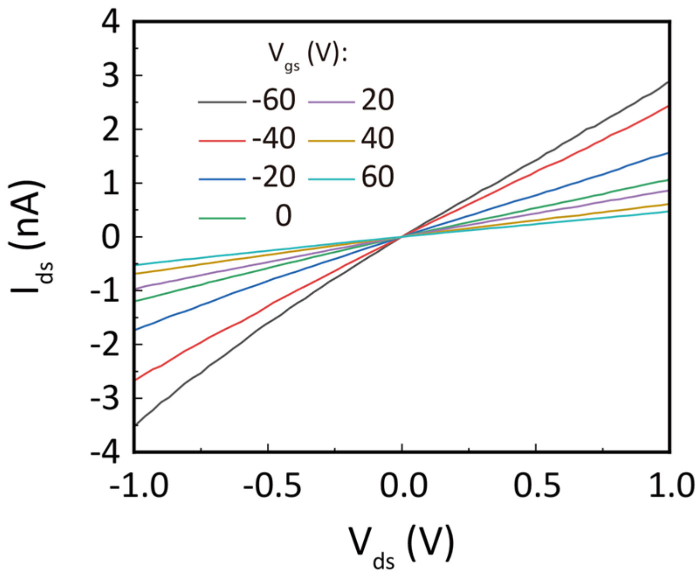

Figure S6. I_{ds}-V_{ds} output characteristics of MnTe-based FET.

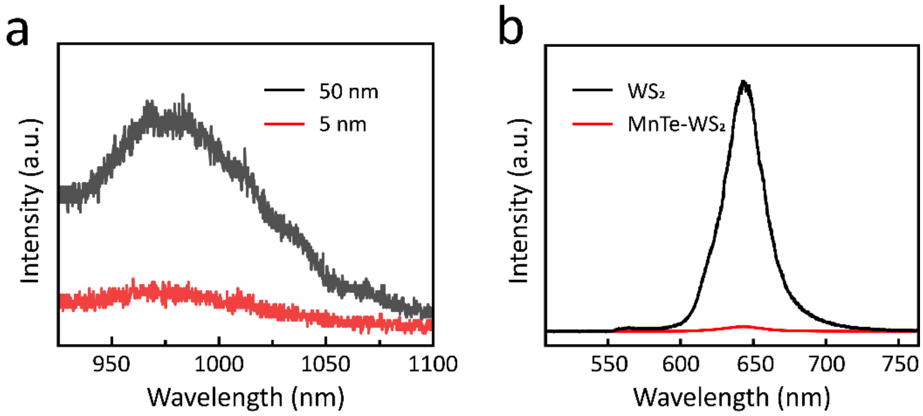

Figure S7. (a)PL spectra of MnTe nanosheets with different thicknesses. (b) PL spectra of a few layers of WS_2 nanosheets and MnTe/WS_2 heterostructure.

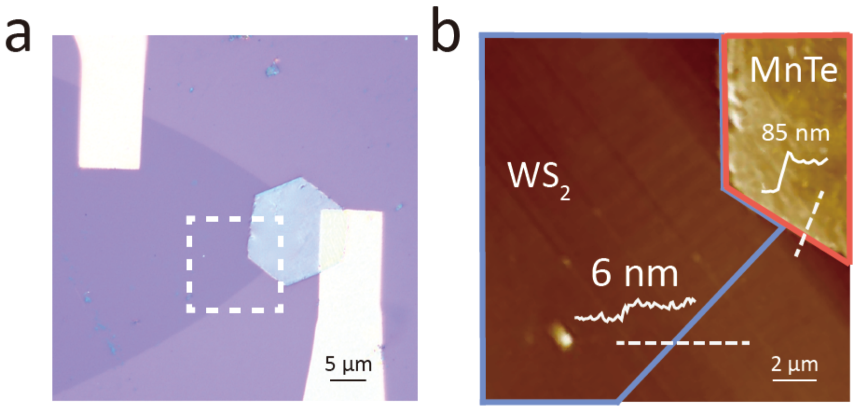

Figure S8. The optical microscopy image (a) and the AFM image (b) of MnTe-WS_2 heterojunction photodetector device.

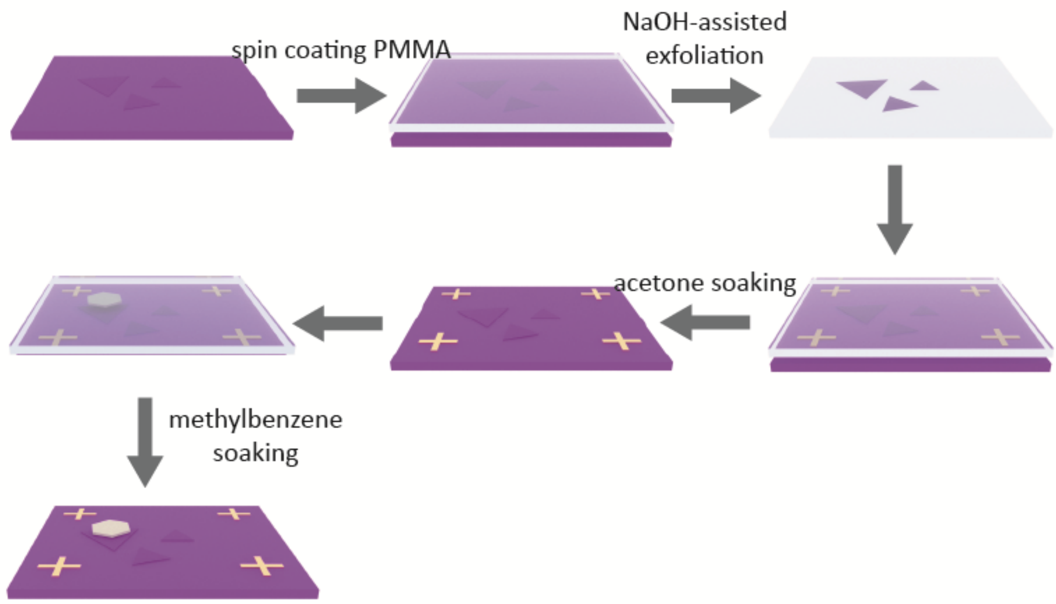

Figure S9. Schematic diagram of the process to fabricate the MnTe/WS_2 photodetector.

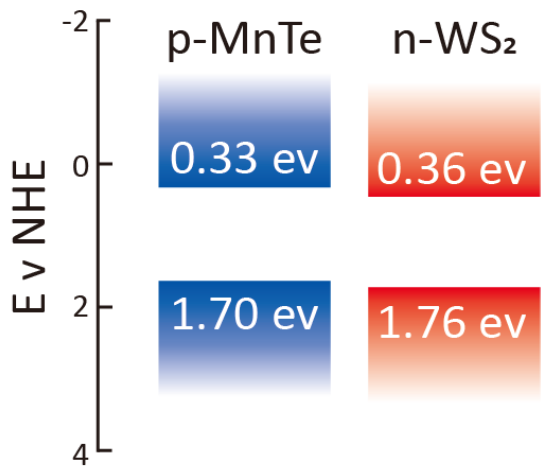

Figure S10. Band alignment of MnTe/WS_2 heterojunction.

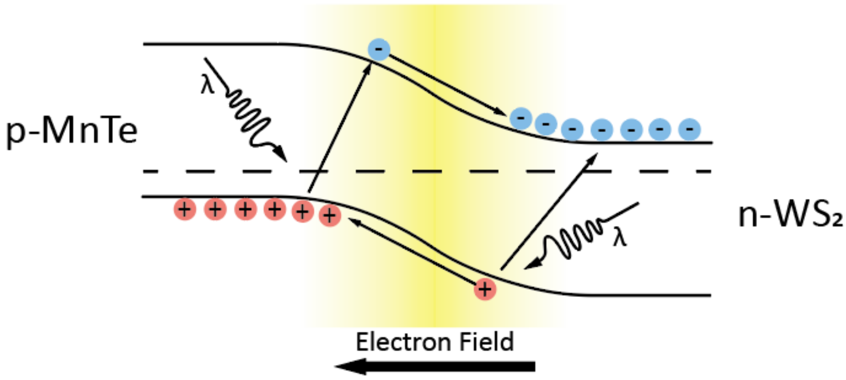

Figure S11. The mechanism diagram of MnTe-WS_2 heterojunction photodetector.

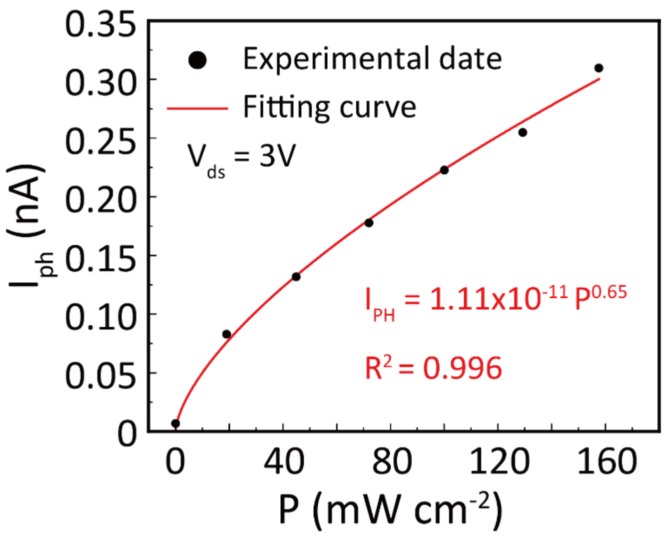

Figure S12. The fitted curve of power density vs. photocurrent.

Table S1. Comparison of the photodetector performance with other 2D heterostructures.

Materials	Method	Wavelength (nm)	Photoresponsivity (A W^{-1})	Detectivity (Jones)	Reference
MnTe/WS_2	CVD-restacking	637	0.271	1.23×10^{10}	This work
WS_2/MoS_2	CVD	532	0.00436	4.36×10^{13}	1
WSe_2/SnS_2	CVD	520	0.108	4.71×10^{10}	2
GaSe/MoS_2	CVD	300	0.065	-	3
GaSe/$MoSe_2$	CVD	white light	0.03	-	4
SnS_2/MoS_2	CVD	638	1.36	-	5
GaSe/Gasb	MBE	637	0.1	2.2×10^{12}	6
ReS_2/$ReSe_2$	Exfoliated-restacking	550	0.021	-	7
$MoTe_2$/MoS_2	Exfoliated-restacking	473	0.06	1.60×10^{10}	8
BP/InSe	Exfoliated-restacking	455	0.017	-	9

References

1 W. Wu, Q. Zhang, X. Zhou, L. Li, J. Su, F. Wang and T. Zhai, *Nano Energy*, 2018, **51**, 45-53.

2 T. Yang, B. Zheng, Z. Wang, T. Xu, C. Pan, J. Zou, X. Zhang, Z. Qi, H. Liu, Y. Feng, W. Hu, F. Miao, L. Sun, X. Duan and A. Pan, *Nat Commun*, 2017, **8**, 1906.

3 N. Zhou, R. Wang, X. Zhou, H. Song, X. Xiong, Y. Ding, J. Lu, L. Gan and T. Zhai, *Small*, 2018, **14**.

4 X. F. Li, M. W. Lin, J. H. Lin, B. Huang, A. A. Puretzky, C. Ma, K. Wang, W. Zhou, S. T. Pantelides, M. F. Chi, I. Kravchenko, J. Fowlkes, C. M. Rouleau, D. B. Geohegan and K. Xiao, *Science Advances*, 2016, **2**, e1501882.

5 B. Li, L. Huang, M. Zhong, Y. Li, Y. Wang, J. Li and Z. Wei, *Advanced Electronic Materials*, 2016, **2**.

6 P. Wang, S. Liu, W. Luo, H. Fang, F. Gong, N. Guo, Z. G. Chen, J. Zou, Y. Huang, X. Zhou, J. Wang, X. Chen, W. Lu, F. Xiu and W. Hu, *Adv Mater*, 2017, **29**.

7 A.-J. Cho, S. D. Namgung, H. Kim and J.-Y. Kwon, *APL Materials*, 2017, **5**.

8 F. Wang, L. Yin, Z. X. Wang, K. Xu, F. M. Wang, T. A. Shifa, Y. Huang, C. Jiang and J. He, *Advanced Functional Materials*, 2016, **26**, 5499-5506.

9 S. Zhao, J. Wu, K. Jin, H. Ding, T. Li, C. Wu, N. Pan and X. Wang, *Advanced Functional Materials*, 2018, **28**.